Philosophical Magazine

ISSN: 1478-6435 (Print) 1478-6443 (Online) Journal homepage: http://www.tandfonline.com/loi/tphm20

MgCu metallic glass

Murat Durandurdu

To cite this article: Murat Durandurdu (2017): MgCu metallic glass, Philosophical Magazine, DOI: 10.1080/14786435.2017.1414325

To link to this article: https://doi.org/10.1080/14786435.2017.1414325

PHILOSOPHICAL MAGAZINE, 2017
https://doi.org/10.1080/14786435.2017.1414325

Taylor & Francis
Taylor & Francis Group

MgCu metallic glass

Murat Durandurdu

Department of Materials Science & Nanotechnology Engineering, Abdullah Gül University, Kayseri, Turkey

ABSTRACT

We generate an amorphous MgCu model using the rapid solidification of the melt through a first-principles molecular dynamics approach within a generalised gradient approximation and reveal, for the first time, its structural features and mechanical properties in details. The liquid and glassy MgCu are found to acquire slightly distinct local structures. Yet in both forms of MgCu, most Cu atoms have a tendency to form the ideal and defective icosahedrons while Mg atoms are arranged in complex configurations. The mean coordination number of Cu and Mg at 300 K is 11.31 and 13.73, respectively. The short-range order of MgCu glass is projected to be different than the known crystalline MgCu and Mg_2Cu phases. The mechanical properties of MgCu glass and the CsCl-type MgCu crystal are computed and compared. On the basis of the enthalpy analyses, a possible pressure-induced crystallisation of the MgCu glass into a CsCl-type structure is proposed to occur at around 11 GPa.

ARTICLE HISTORY
Received 24 August 2017
Accepted 4 December 2017

KEYWORDS
MgCu; metallic glass; phase transformation; *ab initio*; high pressure

1. Introduction

Magnesium (Mg)-based materials have drawn specific interests because of their excellent properties such as lightweight, biocompatibility, electromagnetic shielding, thermal conductivity. To date, different Mg-based intermetallic compounds have been synthesised including Mg–Zn [1], MgCu [2], Mg–Sr [3], Mg–Ca [4], Mg–Ni [5]. However, some of Mg-based alloys show the poor corrosion resistance and low strength, which strictly limit their applications [6,7]. The studies have revealed that the amorphous form of Mg-based materials shows better mechanical properties than their crystalline counterparts [8] and hence, they might offer more high-tech applications than the crystals might.

The glass formation occurs commonly in Mg-rich MgCu binary alloys [9]. The investigations on MgCu systems have exposed that its glass-forming ability and mechanical features can be considerably enhanced by adding small quantity of

CONTACT Murat Durandurdu murat.durandurdu@agu.edu.tr

different kinds of elements [10–16]. Until recently, there has not been any report on the preparation of Cu-rich MgCu amorphous systems because the preparation of such systems requires very fast quenching rates [17]. Chou *et al.* [17] fabricated Cu-rich amorphous MgCu alloys using a co-sputtering method. Ma *et al.* [18] lately investigated the phase development of Mg and Cu (MgCu) systems using a high-energy milling process and reported the formation of an amorphous state after 18 hours of milling.

Although the properties of high-pressure synthesised crystalline MgCu phase having a CsCl structure have been investigated [19], to our knowledge the atomic structure and the properties of amorphous MgCu still remain unidentified. In this study, we perform *ab initio* molecular dynamics (MD) simulations to evaluate its short-range order and mechanical properties in details.

2. Method

The simulations were done using the SIESTA DFT code [20] within the norm-conserving pseudopotentials [21] and a generalised gradient approximation [22]. We used four special **k** points and the double zeta plus polarised orbitals to generate the glass model. We executed the MD simulations within the NPT ensemble. The velocity rescaling approach was adopted to control temperature and the Parrinello-Rahman method [23] was used to equilibrate the volume of the supercell. One femtosecond was chosen for each MD step. We used the CsCl-structured MgCu having 160 atoms as a starting structure. The crystal was exposed to 1500 K for 2.0 ps. After 2.0 ps period, the external temperature was rapidly reduced to 1200 K at which point the structure was equilibrated for 40.0 ps. In order to ensure that we had a liquid state at this temperature, we computed the mean-square displacement (MSD) and offered it in Figure 1. After 200 fs, the MSD

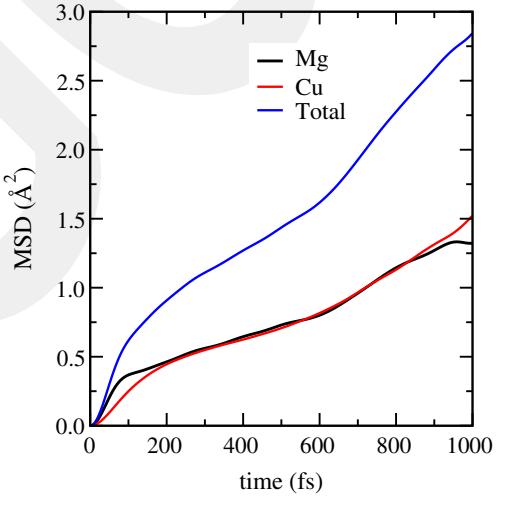

Figure 1. (colour online) Mean-square displacement.

presented a linear behaviour, demonstrating a diffuse state. A linear fit of the diffusive part (200–600 fs) yields the diffusion constant $D(= \langle (r(t) - r(0))^2 \rangle / 6t)$ to be ~2.8 × 10^{-5} cm^2/s for the MgCu liquid, 1.3 × 10^{-5} cm^2/s for Cu atoms and 1.5 × 10^{-5} cm^2/s for Mg atoms. After confirming the liquid state at 1200 K, we reduced the temperature gradually to 300 K in 90 ps. At 300 K, we run additional 5000 time steps. The 1000 configurations of the liquid and amorphous states were used for the structural analyses. The density of the amorphous (300 K) and liquid states (1200 K) is 4.28 and 4.09 g/cm^3, respectively. To calculate the mechanical properties of the crystalline MgCu (CsCl), we used a supercell with 54 atoms and 18 special **k**-points.

3. Results and discussion

3.1. Local structure

The first coordination shell of real space partial-pair distribution functions (PPDFs) offers considerable information regarding the microstructure of disordered materials. Thus, we first evaluate the PPDFs of the liquid MgCu (1200 K) and amorphous MgCu (300 K) phases and demonstrate them in Figure 2. The estimated bond distances (the first peak position of the PPDFs) and some data

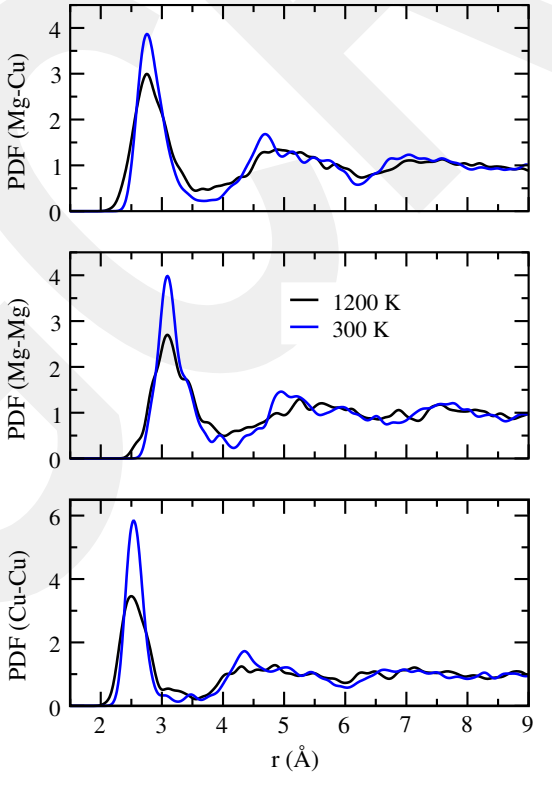

Figure 2. (colour online) Real space partial-pair distribution functions.

available in the Literature are summarised in Table 1. As understood from the table, our values are fairly comparable with other results [14,24,25]. We should note here that the bond lengths of the liquid and amorphous states are too close to each other suggesting that they are not too sensitive to temperature.

One of the most sensitive measures to distinguish the microstructure of disordered systems is total and/or partial coordination numbers (CNs). Therefore, next we examine the partial CNs using the Voronoi polyhedra consideration [26] that is an effective technique to determine accurately CNs. The first minimum of the PPDFs is used for the Voronoi polyhedra investigation. The average Cu–Cu, Cu–Mg, Mg–Cu and Mg–Mg CNs of the amorphous (liquid) structure are 5.27 (5.05), 6.03 (5.91), 6.03 (5.91) and 7.6 (7.35), correspondingly. These partial CNs lead to the mean CN of Cu and Mg atoms to be 11.31 (10.96) and 13.73 (13.26), respectively. Our predictions are reasonably comparable with the earlier simulations' data as exhibited in Table 2. From the partial CN analysis and the chemical environmental distribution of Cu and Mg atoms provided in Table 3, one can see that Cu atoms have an affinity to form less Cu–Cu bonds and lower coordinated configurations than Mg atoms and the average CN of the liquid and amorphous states is comparatively close to each other although they have different types of atomic clusters as seen in Table 3.

Figure 3 shows the coordination distribution of the liquid and amorphous MgCu. In both states, Cu atoms mainly have 10–12 coordinated clusters while Mg atoms have a trend to form 12–15 coordinated configurations. These topological arrangements can be easily characterised by the Voronoi tessellation method [26]. The indices $\langle n_3, n_4, n_5, n_6, \ldots \rangle$ are used to symbolise a Voronoi polyhedron. n_i offers the number of i-edge faces of a polyhedron and $\sum n_i$ gives the total CN. Figure 4 presents the kinds and portions of Cu- and Mg-centred clusters for the structure at 1200 and 300 K. The most common polyhedrons for Cu-centred are $\langle 0\,0\,12\,0\,0 \rangle$ (ideal icosahedron), $\langle 0\,2\,8\,1\,0 \rangle$ (defective icosahedrons), $\langle 0\,2\,8\,2\,0 \rangle$ (distorted icosahedra), $\langle 0\,2\,8\,0\,0 \rangle$ (bicapped square archimedean antiprism), $\langle 0\,3\,6\,1\,0 \rangle$ (defective tri-capped trigonal prism), $\langle 3\,6\,2\,0 \rangle$ (defective fcc like) and $\langle 4\,4\,2\,0 \rangle$ (defective hcp like). In the amorphous state, the perfect or defective icosahedrons are the most privilege clusters for Cu atoms, suggesting a dominated icosahedral-like short-range order around Cu atoms. On the other hand, the clustering around Mg atoms is more complicated and they form 39 and 26 different types of clusters in the liquid and amorphous states, respectively. The polyhedron with the $\langle 0\,1\,10\,2\,0 \rangle$ (defective icosahedrons) index for Mg atoms is the most popular one

Table 1. The nearest neighbour distances of liquid (L) and amorphous (A) MgCu.

	Mg–Mg (Å)	Mg–Cu (Å)	Cu–Cu (Å)	
$Mg_{50}Cu_{50}$ (L)	3.09	2.75	2.50	Present work
$Mg_{50}Cu_{50}$ (A)	3.09	2.75	2.54	Present work
$Mg_{65}Cu_{25}Y_{10}$	3.09	2.71		Ref. [14]
$Mg_{60}Cu_{30}Y_{10}$	2.93	2.72	2.55	Ref. [23]
$Mg_{65}Cu_{25}Gd_{10}$	3.08	2.68	2.48	Ref. [24]

Table 2. The mean CN of Mg and Cu atoms.

	Mg–CN	Cu–CN	
$Mg_{50}Cu_{50}$ (L)	13.26	10.96	Present work
$Mg_{50}Cu_{50}$ (A)	13.73	11.31	Present work
$Mg_{65}Cu_{25}Y_{10}$	13.12	–	Ref. [14]
$Mg_{60}Cu_{30}Y_{10}$	12.7	10.5	Ref. [23]
$Mg_{65}Cu_{25}Gd_{10}$	13.1	9.8	Ref. [24]

Table 3. Chemical environmental distribution of Cu and Mg atoms.

CN	Clusters around Cu	300 K (%)	1200 K (%)	CN	Clusters around Mg	300 K (%)	1200 K (%)
12	Cu_6Mg_6	13.75	10.0	13	Cu_6Mg_7	3.75	6.25
12	Cu_7Mg_5	8.75	8.75	13	Cu_5Mg_8	11.25	5.00
10	Cu_2Mg_8	2.50	2.50	14	Cu_4Mg_{10}	3.75	2.50
10	Cu_3Mg_7	5.00	8.75	13	Cu_4Mg_9	7.50	6.25
12	Cu_4Mg_8	7.50	–	13	Cu_2Mg_{11}	3.75	–
11	Cu_3Mg_8	5.00	2.50	13	Cu_3Mg_{10}	3.75	–
9	Cu_2Mg_7	2.50	2.50	14	Cu_7Mg_7	10.0	11.25
11	Cu_4Mg_7	5.00	6 .25	12	Cu_6Mg_6	2.50	–
11	Cu_6Mg_5	10.0	10.0	14	Cu_6Mg_8	5.00	6.25
10	Cu_5Mg_5	2.50	6.25	15	Cu_7Mg_8	8.75	3.75
11	Cu_5Mg_6	8.75	8.75	12	Cu_4Mg_8	5.00	5.00
12	Cu_8Mg_4	6.25	3.75	14	Cu_8Mg_6	5.00	5.00
13	Cu_7Mg_6	2.50	2.50	14	Cu_9Mg_5	3.75	2.50
12	Cu_5Mg_7	5.00	–	14	$Cu_{10}Mg_4$	2.50	–
11	Cu_7Mg_4	3.75	2.50	14	Cu_5Mg_9	3.75	3.75
10	Cu_4Mg_6	2.50	6.25	13	Cu_7Mg_6	2.50	5.00
9	Cu_3Mg_6	–	3.75	12	Cu_5Mg_7	–	6.25
12	Cu_7Mg_5	–	6.25	15	Cu_5Mg_{10}	–	2.50
				14	Cu_9Mg_5	–	2.50
				12	Cu_7Mg_5	–	3.75

Notes: CN is the coordination number. The clusters having fraction of 2.5% are not listed.

in the amorphous state while the ⟨0 3 6 4 0⟩ index (deformed fcc-like) is the most abundant one in the liquid phase.

Figure 5 shows the positions of Cu- and Mg-centred icosahedrons in the glass model. Most icosahedrons are not randomly distributed and they are indeed linked to each other through vertex, edge, face or intercross sharing. The interconnected icosahedra result in large clusters in the model. Subsequently, the medium range order can be relatated to these icosahedrons as well.

The common neighbor analysis (CNA) [27] can supply valuable information regarding the types of bonding in disordered materials. The analysis ascribes four indices *i*, *j*, *l*, *m* to pair of atoms. The diverse CNA indices denote distinct local structures. The hcp phase has two type pairs, 1421 and 1422. The fcc-type crystal has predominantly 1421 bonding nature. The bcc state has both 1441 and 1661 bond types. The 1551 and 1541 pairs represent the icosahedral ordering and the defected icosahedral ordering, respectively. The 1431 index means fcc-like defects. The 13XX types of bonding correspond to the rhombohedral-like ordering. The 1551, 1541 and 1431 pairs are considered to be the main bonding pairs in disordered materials. The results of CNA are shown in Figure 6. The amorphous model largely presents the 1551 (%30), 1541 (%18), 1431 (%22) and 1422 (11%) bond natures, suggesting

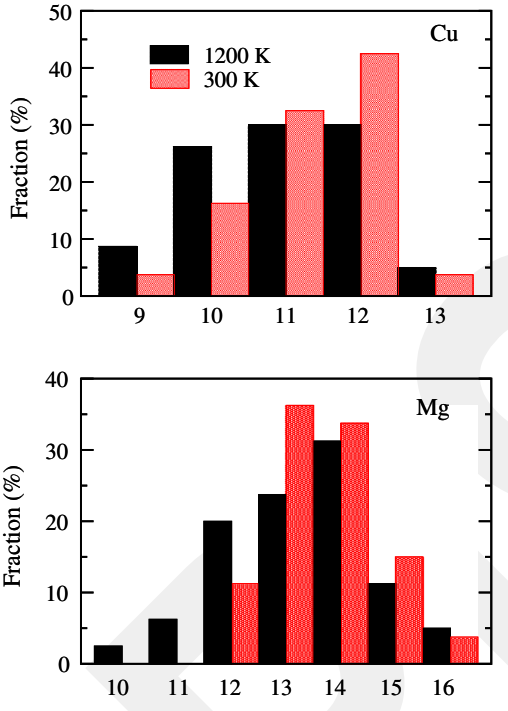

Figure 3. (colour online) Coordination distribution of Cu and Mg atoms.

dominated icosahedral-like, defective fcc-like and hcp-like orderings. Note that the fraction of the bcc-type bonding is negligibly small in the model. In the liquid state, the fcc-like defect (1431) is the leading bonding, and more the rhombohedral-like ordering is presented compared to the amorphous state.

Are there any structural similarities between the glass model and the crystalline phases (CsCl-type MgCu and Mg_2Cu)? The model has negligibly amount of bcc types bonding and no bcc-like polyhedrons ($\langle 0\,6\,0\,8\,0 \rangle$). The Mg_2Cu crystal has two types of the Voronoi clusters $\langle 0\,0\,12\,3\,0 \rangle$ for Mg atoms and $\langle 0\,2\,8\,0\,0 \rangle$ for Cu atoms. The $\langle 0\,2\,8\,0\,0 \rangle$-type cluster does exist in the model but its frequency is only 5%. The $\langle 0\,0\,12\,3\,0 \rangle$ polyhedron also forms in the model but again its fraction is less than 4%. So we conclude that the MgCu metallic glass is locally different than these crystals.

3.2. Mechanical properties

To calculate the bulk modulus (K) that defines the compressibility of materials, the energy of the amorphous model and the CsCl-type MgCu (for comparison purpose) as a function of volume is studied using the conjugant gradient variable cell optimisation technique (both lattice parameters and atomic positions are relaxed), and then the energy-volume data are fit to the third-order Birch-Murnaghan equation of states,

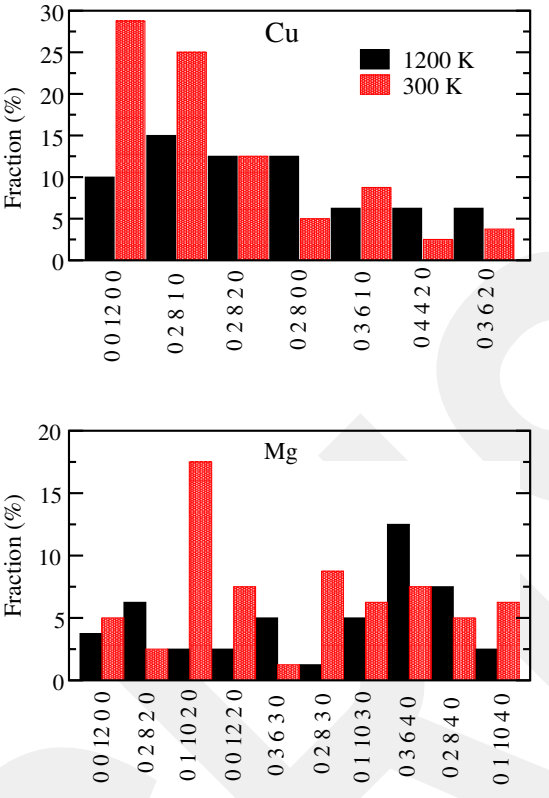

Figure 4. (colour online) Fraction of Cu-and Mg-centred Voronoi polyhedrons. Only polyhedrons having a fraction of 5% and higher are shown in the figure.

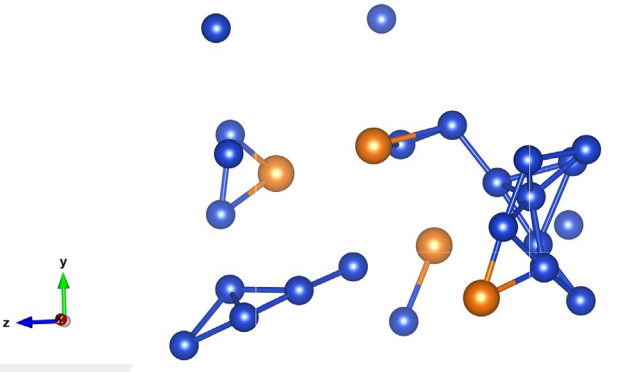

Figure 5. (colour online) Position of ideal icosahedrons centred Cu-and Mg-atoms at 300 K.

$$E(V) = E_o + \frac{9V_O K}{16}\left\{\left[\left(\frac{V_O}{V}\right)^{\frac{2}{3}} - 1\right]^3 K' + \left[\left(\frac{V_O}{V}\right)^{\frac{2}{3}} - 1\right]^2 \left[6 - 4\left(\frac{V_O}{V}\right)^{\frac{2}{3}}\right]\right\}$$

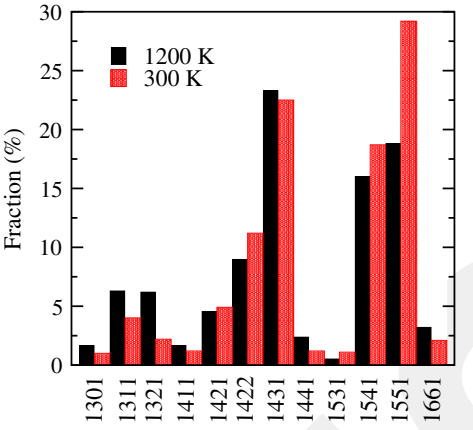

Figure 6. (colour online) Fraction of bond pairs for the liquid state (1200 K) and glass state (300 K).

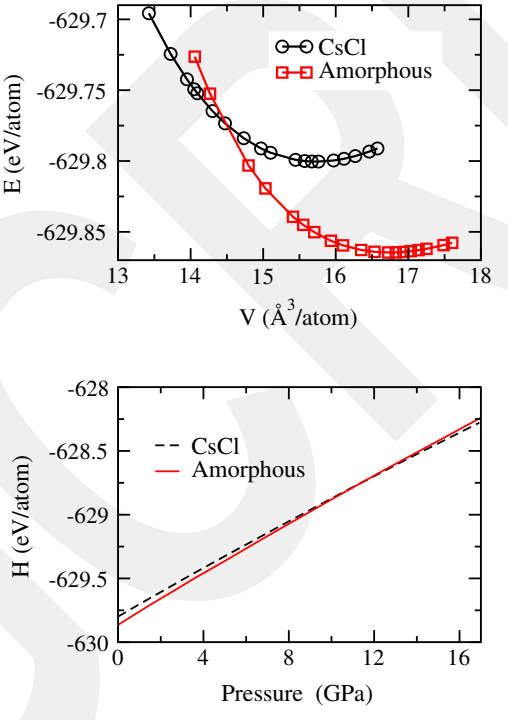

Figure 7. (colour online) Energy-volume relation (top panel). Enthalpy as a function of pressure (bottom panel).

where E and E_0 represent the energy and the equilibrium energy, respectively, V and V_0 is the volume and the equilibrium volume, correspondingly, K is the equilibrium bulk modulus and K' is its derivative respect to pressure. The energy-volume relations are provided in Figure 7. From the figure, one can see that the glass model is energetically more favourable than the crystalline one. The relative energy difference between these structures is 0.064 eV/atom. The equilibrium volume of

the crystal is 15.73 Å^3/atom and the corresponding lattice parameter is about 3.156 Å, in excellent agreement with the experimental and earlier theoretical values of 3.073–3.163 Å [2,18]. The equilibrium volume of the glass is 16.73 Å^3/atom. So the crystal is denser than the glass model. The K value of the CsCl-type phase calculated is 73.3 GPa, which agrees well the other predictions of 68.7–75.25 GPa [2,18]. The bulk modulus of glassy MgCu is estimated to be ~58.2 GPa.

The Gibbs free energy, $G = E + PV - TS$, allows us to determine the stability of different phases of a material. Since our simulations for the optimisation are achieved at zero temperature, the entropic contribution is disregarded such that the Gibbs free energy becomes the static enthalpy $H = E + PV$. We can have pressure (P) by the differentiation of the energy volume curves i.e., $P = -\mathrm{d}E/\mathrm{d}V$. Figure 7 gives the estimated enthalpy values of the glass and crystalline forms of MgCu as a function of pressure. Crossing of two enthalpy curves suggests a potential structural phase transformation between two phases. The two curves cross at around 11 GPa, implying a pressure-induced crystallisation of the MgCu glass into a CsCl-type structure at this pressure. The CsCl phase was experimentally prepared at 800 °C under 6 GPa [2] and thus our transition pressure is in the acceptable limits. This is a first-order phase transformation and involves ~7% volume reduction.

In order to evaluate the Poisson's ratio, we apply a uniaxial stress along one of the diagonal terms of the simulation cell vectors and set the other stress components zero. Both atomic coordinates and simulation cell vectors are optimised. The application of a uniaxial stress frequently leads to an enlargement in the other directions, which is described by the Poisson's ratio defined as:

$$\upsilon_{ij} = -\frac{\Delta L_i/L_i}{\Delta L_j/L_j}$$

where L ($i,j = x,y,z$, j is the compressed direction and i is the transfer directions) are the length of the simulation cell vectors. These procedures are repeated for all three diagonal directions. The variation of $\Delta L_i/L_i$ and $\Delta L_j/L_j$ for some uniaxial compressions is given in Figure 8. The Poisson's ration is estimated from the slope of the best fitting straight line; six different values ranging from 0.12 to 0.33 are achieved for the glass model. The averaged Poisson's ratio is estimated to be 0.18. Due to the cubic symmetry, the crystalline structure is compressed only along x-direction and a value of 0.28 for the Poisson's ratio is acquired, which is objectively comparable with the earlier calculations of 0.27 (GGA-calculation)–0.32 (LDA-calculation) [19]. Note that due to the linear fitting, we certainly anticipate some errors in our estimated Poisson's ratios. Since six different values are projected from the fitting for the glass model, the error is expected to be more for it. Also unlike the crystal, under compression, the simulation cell of the amorphous model undergoes easily deformations (the simulation cell vectors of the amorphous model are not orthogonal). Such a small deformation can yield some errors

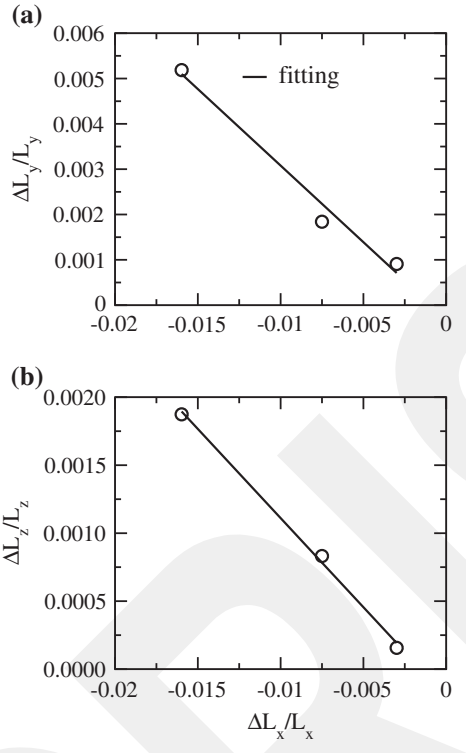

Figure 8. The variation of (a) $\Delta L_y/L_y$ as a function of $\Delta L_x/L_x$ and (b) $\Delta L_z/L_z$ as a function of $\Delta L_x/L_x$. From a linear fit, the Poisson's ratio is estimated to be 0.33 (a) and 0.13 (b).

in our computed Poisson's ratio as well. Consequently we believe that we have some uncertainties in the predicted Poisson's ratio of the glass model.

The Young's modulus (E) expressed as the resistance of a material to elastic deformation under loading is estimated to be 96.4 GPa for the crystal and 111.3 GPa for the glassy MgCu using the following relation:

$$E = 3K(1 - 2\nu).$$

The predicted value for the CsCl phase is in good agreement with the other calculation results of 88 (LDA) and 95 (GGA) [19]. It should be pointed out here that the estimated E value of the glass is fairly close to 96 GPa measured for the amorphous $Mg_{40.4}Cu_{59.6}$ systems [17] as well. The higher Young's modulus of the amorphous phase, relative to the crystal, is probably due to the errors in the Passion's ratio. If we assume that we have no error in our computed the bulk modulus, to have a Young's modulus less than 96.4 GPa for the glass model, its Poisson's ratio must be bigger than 0.225 that we call the corrected Poisson's ratio hereafter.

The shear modulus (μ), determining the stiffness of materials, is projected to be 37.66 GPa for the crystal and 47.1 GPa (39.1 GPa the corrected Poisson's ratio) for the glass state using the following equation:

$$\mu = \frac{E}{2(1+\nu)}$$

where μ was reported to be 55–58 GPa for the CsCl-type phase in the previous investigation [18], which is rather higher than our estimation.

We eventually evaluate the Vickers hardness using Chen's equation [28]

$$H = 2\left(\frac{\mu}{n^2}\right)^{0.585} - 3\,(\text{GPa})$$

where n is the Pugh's ratio ($n = K/\mu$). The hardness is estimated to be 11.98 GPa (less than 7.7 GPa for the corrected Poisson's ratio) for the glass configuration and 4.69 GPa for the crystal structure. The hardness of the amorphous $Mg_{40.4}Cu_{59.6}$ systems was measured to be 4.3 ± 0.1 GPa [17] that is in the range of our predictions.

The Pugh's ratio is linked to brittle or ductile behaviour of materials. If n is higher (less) than1.75, then a material is ductile (brittle). n is 1.22 (1.48 for the corrected Poisson's ratio) for the glass state suggesting its brittle behaviour and it is 1.93 for the CsCl crystal implying its ductile behaviour. In a stark contrast to our prediction, however, the earlier study found n to be in the range of 1.26–1.42 [19] and the crystal is brittle. This controversy can be clarified by additional experiments.

4. Conclusions

We have performed first-principles MD simulations to create a MgCu glass model from its melt and revealed that the liquid and glass forms of MgCu have marginally dissimilar short-range order. In both states, Cu atoms form 10–12 coordinated configurations and most of which are the ideal and defective icosahedrons. Mg atoms, on the other hand, tend to form 12–15 coordinated configurations. The local structure of the amorphous model is different than the crystalline phases. From the enthalpy investigations, we propose a possible pressure-induced phase transformation from the MgCu glass to a CsCl-type structure at about 11 GPa with a first-order nature. The mechanical properties of the crystal and amorphous phases are found to be comparable with each other.

Acknowledgements

The calculations were run on TÜBİTAK ULAKBİM, High Performance and Grid Computing Center (TRUBA resources).

Disclosure statement

No potential conflict of interest was reported by the author.

Funding

This work was supported by the Abdullah Gül University Support Foundation.

References

[1] H. Watanabe, Y. Goto, A. Kamegawa, H. Takamura, and M. Okada, *High pressure synthesis of novel compounds in Mg–TM systems (TM = Ti~Zn)*, Mater. Trans. 45 (2004), pp. 1350–1354.

[2] H. Takamura, H. Kakuta, Y. Goto, H. Watanabe, A. Kamegawa, and M. Okada, *High-pressure synthesis and energetics of MgCu with a CsCl-type structure*, J. Alloys Compd. 404–406 (2005), pp. 372–376.

[3] X. Gu, X. Xie, N. Li, Y. Zheng, and L. Qin, *In vitro and in vivo studies on a Mg–Sr binary alloy system developed as a new kind of biodegradable metal*, Acta Biomater. 8 (2012), pp. 2360–2374.

[4] Z. Li, X. Gu, S. Lou, and Y. Zheng, *The development of binary Mg–Ca alloys for use as biodegradable materials within bone*, Biomaterials 29 (2008), pp. 1329–1344.

[5] A. Kamegawa, Y. Goto, R. Kataoka, H. Takamura, and M. Okada, *High-pressure synthesis of novel compounds in an Mg–Ni system*, Renewable Energy 33 (2008), pp. 221–225.

[6] N. Li and Y. Zheng, *Novel magnesium alloys developed for biomedical application: a review*, J. Mater. Sci. Technol. 29 (2013), pp. 489–502.

[7] X. Zhang, J. Sun, J. Luo, B. Wang, and J. Cheng, *Mechanical and corrosion behaviour of in situ intermetallic phases reinforced Mg-based glass composite*, Mater. Sci. Technol. 33 (2017), pp. 1186–1191.

[8] H.F. Li and Y.F. Zheng, *Recent advances in bulk metallic glasses for biomedical applications*, Acta Biomaterialia 36 (2016), pp. 1–20.

[9] A.A. Nayeb-Hashemi and J.B. Clark, *The Cu-Mg (copper-magnesium) system*, J. Phase Equilib. 5 (1984), pp. 36–43.

[10] A. Inoue, *Bulk amorphous and nanocrystalline alloys with high functional properties*, Mater. Sci. Eng. A 304–306 (2001), pp. 1–10.

[11] Q. Zheng, H. Ma, E. Ma, and J. Xu, *Mg–Cu–(Y, Nd) pseudo-ternary bulk metallic glasses: the effects of Nd on glass-forming ability and plasticity*, Scr. Mater. 55 (2006), pp. 541–544.

[12] E.S. Park, H.G. Kang, W.T. Kim, and D.H. Kim, *The effect of Ag addition on the glass-forming ability of Mg–Cu–Y metallic glass alloys*, J. Non-Cryst. Solids 279 (2001), pp. 154–160.

[13] H. Ma, L.L. Shi, J. Xu, Y. Li, and E. Ma, *Discovering inch-diameter metallic glasses in three-dimensional composition space*, Appl. Phys. Lett. 87 (2005), pp. 181915–181917.

[14] X. Hui, R. Gao, G.L. Chen, S.L. Shang, Y. Wang, and Z.K. Liu, *Short-to-medium-range order in Mg65Cu25Y10 metallic glass*, Phys. Lett. A 372 (2008), pp. 3078–3084.

[15] H. Men and D.H. Kim, *Fabrication of ternary Mg–Cu–Gd bulk metallic glass with high glass-forming ability under air atmosphere*, J. Mater. Res. 18 (2003), pp. 1502–1504.

[16] Dmitri V. Louzguine, Larissa V. Louzguina, and Akihisa Inoue, *Multistage devitrification of Mg–Ni–Mm and g–Ni–Y–Mm metallic glasses (Mm = Misch metal)*, Philos. Mag. 83 (2003), pp. 203–216.

[17] H.S. Chou, J.C. Huang, Y.H. Lai, L.W. Chang, X.H. Du, J.P. Chu, and T.G. Nieh, *Amorphous and nanocrystalline sputtered Mg–Cu thin films*, J. Alloys Compd. 483 (2009), pp. 341–345.

[18] Z. Ma, Y. Liu, L. Yu, and Q. Cai, *Investigation of phase composition and nanoscale microstructure of high-energy ball-milled MgCu sample*, Nanoscale Res. Lett. 7 (2012), pp. 390–394.

[19] S. Boucetta and F. Zegrar, *Density functional study of elastic, mechanical and thermodynamic properties of MgCu with a CsCl-type structure*, J. Magnesium Alloys 1 (2013), pp. 128–133.

[20] P. Ordejón, E. Artacho, and J.M. Soler, *Self-consistent order-N density-functional calculations for very large systems*, Phys. Rev. B 53 (1996), pp. R10441–R10444.

[21] N. Troullier and J.M. Martins, *Efficient pseudopotentials for plane-wave calculations*, Phys. Rev. B 43 (1991), pp. 993–2006.
[22] J.P. Perdew, K. Burke, and M. Ernzerhof, *Generalized gradient approximation made simple*, Phys. Rev. Lett. 77 (1996), pp. 3865–3868.
[23] M. Parrinello and A. Rahman, *Polymorphic transitions in single crystals: a new molecular dynamics method*, J. Appl. Phys. 52 (1981), pp. 7182–7190.
[24] P. Jóvári, K. Saksl, N. Pryds, B. Lebech, N.P. Bailey, A. Mellergad, R.G. Delaplane, and H. Franz, *Atomic structure of glassy Mg60Cu30Y10 investigated with EXAFS, X-ray and neutron diffraction, and reverse Monte Carlo simulations*, Phys. Rev. B 76 (2007), pp. 42–054216.
[25] D. Liu, S.P. Pan, J.Y. Qin, and T.K. Gu, *Chemical and topological short-range order evolution of Mg65Cu25Gd10 alloy in the process of rapid solidification*, J. Appl. Phys. 109 (2011), pp. 093519–093524.
[26] N.N. Medvedev, *The algorithm for three-dimensional Voronoi polyhedral*, J. Comput. Phys. 67 (1986), pp. 223–229.
[27] J.D. Honeycutt and H.C. Andersen, *Molecular dynamics study of melting and freezing of small Lennard-Jones clusters*, J. Phys. Chem. 91 (1987), pp. 4950–4963.
[28] X.Q. Chen, H. Niu, D. Li, and Y. Li, *Modeling hardness of polycrystalline materials and bulk metallic glasses*, Intermetallics 19 (2011), pp. 1275–1281.